Impact of Mn(II)-Manganese Oxide Reactions on Ni and Zn Speciation

Margaret A. G. Hinkle*, Katherine G. Dye† and Jeffrey G. Catalano

Department of Earth and Planetary Sciences, Washington University, 1 Brookings Drive, Saint Louis, MO 63130 USA

*Corresponding author: Tel.: +1-202-633-1815; Fax: +1-202-357-2476; E-mail: mhinkle@eps.wustl.edu

Word count with text (abstract through acknowledgements: 5,352 words), figures (1200 words), and tables (600 words) is 7,152 words

Submitted to *Environmental Science & Technology*

August 2016
Revised December 2016
Revised February 2017

ABSTRACT

Layered Mn oxide minerals (phyllomanganates) often control trace metal fate in natural systems. The strong uptake of metals such as Ni and Zn by phyllomanganates results from adsorption on or incorporation into vacancy sites. Mn(II) also binds to vacancies and subsequent comproportionation with structural Mn(IV) may alter sheet structures by forming larger and distorted $Mn(III)O_6$ octahedra. Such Mn(II)-phyllomanganate reactions may thus alter metal uptake by blocking key reactive sites. Here we investigate the effect of Mn(II) on Ni and Zn binding to phyllomanganates of varying initial vacancy content (δ-MnO_2, hexagonal birnessite, and triclinic birnessite) at pH 4 and 7 under anaerobic conditions. Dissolved Mn(II) decreases macroscopic Ni and Zn uptake at pH 4 but not pH 7. Extended X-ray absorption fine structure spectroscopy demonstrates that decreased uptake at pH 4 corresponds with altered Ni and Zn adsorption mechanisms. These metals transition from binding in the interlayer to sheet edges, with Zn increasing its tetrahedrally-coordinated fraction. These effects on metal uptake and binding correlate with Mn(II)-induced structural changes, which are more substantial at pH 4 than 7. Through these structural effects and the pH-dependence of Mn(II)-metal competitive adsorption, system pH largely controls metal binding to phyllomanganates in the presence of dissolved Mn(II).

1. INTRODUCTION

Manganese oxides are highly reactive minerals with a wide occurrence in marine, lacustrine, riverine, and cave systems, acting as metal scavengers.[1-9] As a result of their large adsorption capacities and redox behavior, manganese oxides exert substantial controls on the concentrations and speciation of many trace metals, notably Ni and Zn.[4,9-13] The reactivity of these minerals is largely controlled by their structure,[14-16] which can be affected by cation adsorption onto and incorporation into manganese oxides.[17-27]

Unlike most dissolved cations, the structural effects of dissolved Mn(II) when it reacts with manganese oxides involves both adsorption and comproportionation with Mn(IV), producing solid-phase Mn(III). Recent research shows that Mn(II) promotes the phase transformation of layered Mn(IV/III) oxides (phyllomanganate) into manganite (γ-MnOOH) and hausmannite (Mn_3O_4), involving a feitknechtite (β-MnOOH) intermediary.[28-30] While such transformations affect trace metal speciation,[31] the resulting lower-valent mineral phases are uncommon in environmental systems, which are typically dominated by Mn(IV/III) phyllomanganates,[3,32-37] and these phase transformations may not be widespread in nature. At lower Mn(II):Mn(IV) ratios phase transformations do not occur, with phyllomanganates instead exhibiting modifications to their sheet structures and layer stacking.[21,38-40] pH, reaction time, and the initial manganese oxide composition and structure affect the extent and nature of these Mn(II)-induced modifications.[28,30,39,40]

The effects of Mn(II) on phyllomanganates suggest that metals may display altered sorption behavior to such minerals in regions with coexisting aqueous Mn(II), such as at redox interfaces in soils, sediments, and water columns, acid and coal mine drainage remediation sites, or regions with active biogeochemical manganese cycling. Many cations bind in the interlayer of

phyllomanganates by adsorbing over vacancy sites,[41-49] although edge sites remain highly reactive towards adsorbates in Mn(III)-rich phyllomanganates.[16,50-53] Over time, structurally compatible cations like Ni become progressively incorporated into the phyllomanganate sheet at these vacancies.[41] Because Mn(II) also binds to these sites,[21,40,49,54] it may alter metal adsorption and subsequent incorporation through site competition and vacancy filling.

In this study, the effects of Mn(II) on Ni and Zn sorption behaviors on phyllomanganates are examined. Mineral vacancy content and pH are hypothesized to be principal factors, as metals typically adsorb over vacancies, exhibiting increased uptake with increasing pH,[35,41,42,44,55] and both vacancy content and pH are important controls on Mn(II)-induced phyllomanganate structural changes.[40] Thus, the manganese oxides examined in this study were selected to explore how vacancies and Mn(III) content affect metal binding: δ-MnO_2 (the synthetic analogue of vernadite) has charge primarily from sheet vacancies, triclinic birnessite has layer charge predominantly from Mn(III) substitutions, and c-disordered H^+ birnessite (a birnessite with hexagonal symmetry) contains both vacancies and Mn(III) substitutions.[56,57] Acidic and neutral pH systems were chosen to reduce the risk of secondary manganese oxide mineral precipitation, which is promoted by higher pH, and because these pH regimes are relevant for natural and polluted systems with coexisting dissolved Mn(II), manganese oxides, and trace metals.[32,45,58-61] Ni and Zn binding mechanisms onto these phyllomanganates during adsorption on and coprecipitation with phyllomanganates were assessed with X-ray absorption fine structure (XAFS) spectroscopy. The effect of the absence and presence of dissolved Mn(II) during aging for 25 days on Ni and Zn uptake and binding mechanisms was also investigated.

2. METHODS AND MATERIALS

2.1. Molecular-Scale Ni and Zn Sorption Experiment Sample Preparation

Ni and Zn sorption onto three different minerals, δ-MnO_2, c-disordered H^+ birnessite (termed 'HexB' in this paper), and triclinic birnessite ('TriB'), in the presence and absence of Mn(II) was investigated by Ni and Zn K-edge XAFS spectroscopy. Mineral syntheses and reagent preparation are described in the SI. δ-MnO_2, HexB, and TriB were previously determined to have ~1±1%, 10±2%, and 40±10% of structural Mn as Mn(III).[40] Samples consisted of 2.5 g L^{-1} δ-MnO_2, TriB, or HexB reacted in a solution containing 0.23 mM Ni(II) or Zn(II) with 10 mM NaCl (an ionic strength buffer), 1 mM 2-(4-morpholino)ethanesulfonic acid (MES) buffer (for pH 7 samples), and 0, 0.75, or 7.5 mM Mn(II) for 25 days (as listed in Tables 1 and 2) within an anaerobic chamber (Coy Laboratory Products, Inc., 3% H_2/97% N_2 atmosphere with Pd catalysts) at pH 4 and pH 7. These experiments have Ni(II) and Zn(II):solid Mn(IV) ratios of 0.013-0.016 mol:mol and Ni(II) and Zn(II):solid Mn(total) ratios of 0.009-0.014 mol:mol (using solid Mn(IV) per g mineral and solid Mn(total) per g mineral, respectively, as obtained for the same starting materials and published previously[40]). The Mn(II):solid Mn(IV) ratios are 0.042-0.054 and 0.425-0.543 mol:mol for the 0.75 and 7.5 mM experiments, respectively. The 7.5 mM Mn(II) experiments were conducted at pH 4 only, as feitknechtite precipitation occurs at this Mn(II):Mn(IV) ratio at pH 7[40] and the impact of such phase transformations on trace metal speciation has been previously studied.[31] After the mineral suspension was added to the samples, marking the start of the experiment, the samples were allowed to equilibrate for approximately 1 hour, at which point the pH of the samples was adjusted to pH 4 or 7 with HCl and NaOH. The samples were placed on end-over-end rotators wrapped in aluminum foil. Sample pH was checked, and adjusted if necessary, throughout the duration of the experiment. At the end of the experiment, the samples were filtered (reusable

114 syringe filter; 0.22 μm MCE membrane; Fisher Scientific), discarding the first 1 mL of filtrate
115 and collecting the solid as a wet paste. The filtrates were removed from the anaerobic chamber
116 and promptly acidified to 2% HNO_3 (trace metal grade; OmniTrace® Ultra^{TM}). The acidified
117 filtrates were diluted with 2% HNO_3 for inductively coupled plasma-optical emission
118 spectroscopy (ICP-OES; Perkin Elmer Optima 7300 DV) analysis for dissolved Ni, Zn, and Mn
119 concentrations. Uncertainty (95% confidence level) was determined using the standard
120 deviations from the triplicate instrument analyses. Similar experiments were also conducted to
121 assess the effect of Mn(II) on macroscopic Ni adsorption on short time-scales; experiment details
122 are described in the SI.
123 Additional Mn(II)-free samples of Ni and Zn adsorbed onto phyllomanganates, reacted
124 for just 40 hours, were also prepared for XAFS spectroscopic measurements. These 40 hour
125 samples involved the same experimental parameters described above. Phyllomanganates
126 coprecipitated with Ni and Zn were also analyzed by XAFS spectroscopy. These samples were
127 synthesized following the procedures described in the SI for metal-free phyllomanganates, but
128 with Ni(II) or Zn(II) (using a $NiCl_2$•$6H_2O$ or $ZnCl_2$) substituting for a portion of the
129 $MnCl_2$•$4H_2O$ starting solution [Ni:Mn and Zn:Mn= 0.02]. All syntheses were successful in
130 producing the intended phyllomanganate with approximately 2 mol% Ni (specifically, 1.7 mol%
131 for δ-MnO_2, 1.5 mol% for HexB, 2.1 mol% for TriB) or Zn (2.0 mol% for δ-MnO_2, 0.6 mol% for
132 HexB), with the exception of Zn-coprecipitated TriB. All attempts to synthesize
133 Zn-coprecipitated TriB resulted in the formation of a triclinic birnessite-hetaerolite mixture, even
134 at lower initial Zn contents (e.g., 0.2 mol% Zn), as evidenced by X-ray diffraction (XRD)
135 (Bruker D8 Advance X-ray diffractometer, Cu K_α radiation) patterns and X-ray absorption near
136 edge structure (XANES) spectra (not shown). The precipitation of hetaerolite ($ZnMn_2O_4$)

appears to be favored in systems with substantial Mn(III) contents, as hetaerolite formation was previously observed upon the addition of Zn during the Mn(II)-induced phase transformation of a hexagonal birnessite to feitknechtite.[31]

XAFS samples for the solids (as wet pastes) were prepared following methods described previously.[40] Samples preparation was timed to minimize risk of drying: samples were prepared a maximum of 68 hours prior to the start of experiments for those analyzed at the Advanced Photon Source (APS) at Argonne National Laboratory and 120 hours prior to the start of experiments at the Stanford Synchrotron Radiation Lightsource (SSRL) at the SLAC National Accelerator Laboratory. To preserve anoxic conditions and further prevent drying, each sample was individually sealed in a polyethylene bag with a damp Kimwipe.

2.2. XAFS Spectroscopic Measurements

XAFS spectra were collected at APS beamline 20-BM-B and SSRL beamline 4-1. Beamline 20-BM-B uses a Si (111) fixed-offset double-crystal monochromator, detuned by 10% to attenuate harmonics. Rh-coated Si mirrors were used for focusing and further harmonic rejection. Fluorescence yield Ni and Zn K-edge XAFS spectra were collected with a 12-element energy dispersive solid-state Ge array detector. Beamline 4-1 uses a Si (220) double crystal monochromator, which was detuned by 40% to attenuate beam harmonics. Fluorescence yield Ni and Zn K-edge XAFS spectra were collected using 15 elements of an energy dispersive solid-state Ge array detector. Spectra of Ni and Zn metal foils were used to calibrate the incident beam energy, with the maximum in the first derivative of the K-edges set to 8333 eV and 9659 eV, respectively.

2.3. XAFS Fitting

The Athena[62] graphical user interface to IFEFFIT[63], in conjunction with SamView via the SixPack interface[64] were used to average, process, deadtime correct, and normalize the XAFS spectra. SixPack was also used for spectral fitting, largely following models described in past research[20,35,41,43] for Ni and Zn adsorption onto phyllomanganates. The chalcophanite structure[65] was used to calculate backscattering phase and amplitude functions for the Zn system using FEFF 9.6[66], and Ni substituted for Zn within the chalcophanite structure was used to calculate these functions for the Ni system. The k^3-weighted extended X-ray absorption fine structure (EXAFS) spectra were fit over a k range of 3 – 11.1 $Å^{-1}$ and an R range of 1 – 4.0 Å, with the amplitude reduction factor (S_0^2) fixed to 0.94 for all Ni samples[20] and 0.86 for all Zn samples.[44] Details regarding the structural model fits to the data and the constraints applied to some parameters are provided in the SI.

3. RESULTS

3.1. Effect of Adsorption versus Coprecipitation on Metal Binding Mechanisms

Aging phyllomanganates can involve structural changes [both in the absence and presence of Mn(II)],[39,40,49,54,67-69] thus to better constrain our interpretation of Ni and Zn speciation in this system, we first characterized the Ni and Zn binding modes after 40 hours of reaction with pre-formed phyllomanganates in the absence of Mn(II) and after coprecipitation with the Mn oxides. These two sets of experiments provide a baseline of metal binding by simple adsorption and by coprecipitation during phyllomanganate formation, respectively, and their EXAFS fitting results provide parameter constraints for aged samples (see SI for details).

183 *3.1.1. Metal Adsorption at pH 4*

184 EXAFS spectroscopy shows that Ni and Zn adsorption mechanisms vary substantially
185 with manganese oxide structure. The EXAFS spectra of Ni adsorbed to all three
186 phyllomanganates after 40 hours of reaction at pH 4 (Figure 1) exhibit clear peaks in the Fourier
187 transform at ~3.1 Å, corresponding to double-corner (DC) or triple-corner (TC) sharing surface
188 complex.[35,41] These types of complexes have similar Ni-Mn interatomic distances of ~3.48 Å,
189 which yield a ~3.1 Å feature in the Fourier transform, but the TC complexes have ~6 Mn
190 neighbors because they adsorb above sheet vacancies[20] while the DC complexes have only ~2
191 Mn neighbors because they adsorb at sheet edges. Fitting these spectra (Figure S1) obtains large
192 CNs for the Ni-$Mn_{DC/TC}$ shell (Table S1), indicating that the adsorbed Ni occurs predominantly
193 as TC complexes. The Fourier transform feature at ~5.0 Å confirms that Ni binds as a TC
194 complex as it is associated with a second shell of Mn neighbors present when Ni binds on top of
195 a vacancy site.[20,41,42,55] This feature is generally not observed for DC complexes[20] because of the
196 fewer neighbors involved and greater disorder associated with fewer bonds between Ni and the
197 Mn oxide surface. In addition to features associated with a TC complex, the EXAFS spectrum of
198 Ni adsorbed on TriB at pH 4 also contains peaks in the Fourier transform at ~2.4 Å and 5.5 Å
199 (Figure 1F). These features indicate that a fraction of the solid-bound Ni is incorporated into the
200 phyllomanganate sheet,[35,41-43,55] confirmed by the spectral fit, which includes Ni-Mn shells at
201 2.88 Å, 5.00 Å, and 5.97 Å with CNs of 0.8 (Table S1).

202 Adsorbed Zn binds to δ-MnO_2 and TriB through similar mechanisms as Ni, with the
203 exception that Zn does not incorporate into phyllomanganate sheets and occurs as both
204 octahedral and tetrahedral surface species. These two coordination states can be differentiated by
205 their Zn-O and Zn-Mn interatomic distances [Zn-O = ~2.10 Å (^{VI}Zn) or ~1.97 (^{IV}Zn); TC Zn-Mn

= ~3.50 Å (^{VI}Zn) or ~3.35 Å (^{IV}Zn)].[35,44,70] Intermediate values (e.g., Zn-O distance of ~2.07 Å and Zn-Mn distance of ~3.47 Å) are indicative of mixed but spectrally unresolved tetrahedral and octahedral Zn contributions.[44] ^{VI}Zn can also be visually differentiated from ^{IV}Zn in an EXAFS spectrum, with ^{VI}Zn exhibiting distinct positive antinodes at k = ~3.8 and ~6.1 Å^{-1}, while these are shifted to k = ~4.4 and ~6.4 Å^{-1} for ^{IV}Zn.[18] In samples containing a mixture of ^{VI}Zn and ^{IV}Zn, these features in the EXAFS spectra become dampened and broadened due to overlapping spectral contributions. ^{VI}Zn is favored over ^{IV}Zn at high Zn loadings and in phyllomanganates with strong sheet stacking.[18,70,71]

Such intermediate spectral features are common for Zn adsorbed to phyllomanganates (Figure 2). Similar to Ni, TC and DC Zn complexes are present, both with Zn-Mn interatomic distances at ~3.49 Å. Zn TC and DC complexes can be differentiated as discussed above with Ni. On δ-MnO_2 at pH 4, spectral fits (Figure S2) show that Zn speciation is dominated by TC complexes (Table S2); both tetrahedral and octahedral complexes are present. Zn adsorbed to HexB at pH 4 forms both DC and TC surface complexes, with both tetrahedral and octahedral forms present but unresolvable (Table S2). On TriB, Zn forms TC complexes at pH 4, occurring as both tetrahedral and octahedral species.

3.1.2. Metal Adsorption at pH 7

At pH 7, Ni forms both incorporated and TC species on δ-MnO_2, consistent with past research finding that Ni incorporates into vacancy-rich phyllomanganate sheets as pH increases.[35,41,42,55] In contrast, Ni binds to HexB at pH 7 as predominantly a TC complex (Table S1). Ni adsorption mechanisms on TriB at pH 7 are also distinct, forming both a DC and tridentate edge-sharing (TE) complex (Table S1). TE complexes have been previously identified

229 in Ni-triclinic birnessite systems at circumneutral pH[20,42,50] and have Ni-Mn interatomic
230 distances intermediate between incorporated species and TC or DC complexes.
231 Like Ni, TC Zn complexes form on δ-MnO_2 at pH 7 (Table S2), with ^{IV}Zn and ^{VI}Zn both
232 contributing to the EXAFS spectra (Figure 2). For HexB, the ^{IV}Zn and ^{VI}Zn spectral contributions
233 can be resolved, and the CNs for Mn neighbors indicate a mixture of DC and TC complexes
234 (Table S2), similar to Zn speciation at pH 4. Both ^{IV}Zn and ^{VI}Zn species form on TriB at pH 7,
235 with DC (as ^{IV}Zn and possibly ^{VI}Zn) and TE (as ^{VI}Zn) complexes present (Table S2).
236
237 *3.1.3. Metal Coprecipitation with Phyllomanganates*
238 Ni speciation when coprecipitated with phyllomanganates has much larger fractions of
239 incorporated Ni (Figure 1), with the adsorbed Ni fraction behaving most similar to Ni at pH 4
240 (Table S1). The adsorbed Ni in the coprecipitation samples are likely mixtures of TC and DC
241 complexes, based on the CN values (2.6-5.5) for the ~3.48 Å Ni-Mn shell (Table S1). The
242 fraction of Ni that is incorporated or adsorbed does not vary systematically among the three
243 phyllomanganates studied.
244 Zn binding in the coprecipitated samples, like the adsorbed samples, is also limited to
245 adsorption, with no evidence of incorporation into the phyllomanganate sheets (Figure 2). This is
246 consistent with past work which has found that Zn does not enter vacancy sites,[44,46,70,72] even in
247 the Zn-bearing phyllomanganate mineral chalcophanite.[65] Recent density functional theory
248 calculations suggest that this lack of incorporation is the result of the large size of Zn octahedra,
249 which would cause greater stress on phyllomanganate sheets than can be compensated by
250 structural distortions.[73] Structural models consisting of adsorbed DC and TC Zn species in mixed

coordination states (Table S2) reproduce the EXAFS spectra of Zn coprecipitated with δ-MnO_2 and HexB (Figure S2).

3.2. Effect of Aging and Mn(II) on Metal Binding Mechanisms

3.2.1. pH 4

XANES and EXAFS spectra show that the speciation of Ni adsorbed to phyllomanganates is unaffected by aging for 25 days at pH 4 in the absence of Mn(II) (Figure 1). Similarly, XANES spectra indicate that Zn speciation is unchanged after 25 days of aging without added Mn(II) at pH 4 (Figure 2); EXAFS spectra were not collected for these conditions. Aged samples prepared with added aqueous Mn(II) at pH 4, however, display altered Ni and Zn binding mechanisms, with macroscopic metal uptake correspondingly reduced for most conditions (Table 1). For δ-MnO_2, Ni and Zn binding mechanisms (Figures 1,2) and macroscopic uptake (Table 1) only change when 7.5 mM Mn(II) is added; 0.75 mM Mn(II) does not induce any observable differences. A decrease in the CNs associated with the Ni-Mn and Zn-Mn shells at ~3.48Å (Tables S1,S2) indicates that 7.5 mM Mn(II) promotes a transition from TC to DC complexes for both metals. In addition, the Zn EXAFS spectrum (Figure 2) shows an increased splitting in the 6.1 $Å^{-1}$ antinode, indicating that this Mn(II) concentration increases the proportion of ^{IV}Zn,[18,44] which is supported by the fitting results (Table S2).

In the HexB system, a similar Mn(II)-induced promotion of DC Ni and Zn complexes and of ^{IV}Zn over ^{VI}Zn is observed. For Ni, the Fourier transform feature at ~3.1 Å decreases in amplitude (Figure 1D) with increasing aqueous Mn(II) concentration, consistent with a conversion from a TC complex to a DC complex. With 7.5 mM Mn(II) some Ni also incorporates into HexB. Zn predominantly adsorbs as a DC complex onto HexB (Table S2), with

a greater dissolved Mn(II) concentration promoting ^{IV}Zn over ^{VI}Zn species. These changes to Ni and Zn speciation on HexB at pH 4 in the presence of dissolved Mn(II) are accompanied by decreasing macroscopic uptake (Table 1).

Aqueous Mn(II) also appears to alter Ni and Zn speciation on TriB, but with different effects at low and high initial Mn(II) concentrations. It should be noted that dissolved Mn(II) concentrations in the TriB system were larger than the initial Mn(II) added (Table 1), indicating that structural Mn(III) disproportionates and releases Mn(II) to solution.[40] For Ni, when aged without dissolved Mn(II) or with 7.5 mM Mn(II), similar portions of the solid-associated metal are incorporated into the mineral, but such species are undetectable for the 0.75 mM Mn(II) sample (Table S2). However, the Fourier transform feature at ~3.1 Å (Figure 1I) indicates that the proportion of TC complexes is approximately constant among all Mn(II) concentrations. These changes in speciation do not correlate with macroscopic Ni uptake, which decreases only when 7.5 mM Mn(II) is added (Table 1). Like Ni, macroscopic Zn uptake on TriB also substantially decreases in the presence of 7.5 mM Mn(II) at pH 4. Unlike Ni, however, the addition of dissolved Mn(II) at pH 4 causes a shift from TC to DC surface complexes for Zn (Figure 2). This shift in binding occurs progressively as Mn(II) concentration increases and is accompanied by an increase in the proportion of ^{IV}Zn (Table S2).

3.2.2. pH 7

In contrast to pH 4, Mn(II) has a muted effect on Ni and Zn behavior on phyllomanganates at pH 7. No detectable suppression of macroscopic Ni and Zn sorption by Mn(II) occurs (Table 2). However, both the metals and Mn(II) show complete uptake on all

manganese oxides, suggesting that these adsorbates did not saturate the binding capacity of the solids; competitive effects are thus not expected to be observed for the conditions studied.

Although not affecting uptake, the addition of 0.75 mM Mn(II) during aging at pH 7 alters Ni and Zn solid-phase speciation. The Fourier transform feature associated with incorporated Ni decreases for δ-MnO_2 in the presence of Mn(II) (Figure 1C). Fitting a structural model to the data confirms that incorporated Ni decreases in abundance while TC complexes are unaffected (Table S1). Unlike for Ni, aging Zn with δ-MnO_2 for 25 days at pH 7 alters the spectral features associated with TC and DC surface complexes (Figure 2). Fitting the spectra of Zn bound to δ-MnO_2 indicates that the relative amount of TC and DC complexes is statistically invariant and suggests that the primary speciation change is in the ratio of ^{VI}Zn and ^{IV}Zn.

For HexB, the contribution to the EXAFS spectra of Mn neighbors associated with incorporated Ni is near the limit of detection given the presence of other neighboring shells. While fitting shows that inclusion of such shells in a structural model is only statistically justified for HexB aged in the presence of Mn(II) and not in its absence (Table S1), the Fourier transform feature near ~2.4 Å visually appears unchanged (Figure 1F). It is thus likely that a small fraction of solid-associated Ni is incorporated into the phyllomanganate sheet after 25 days of reaction at pH 7, even in the absence of Mn(II). TC surface complexes are also present and remain unaffected by Mn(II) addition. Similarly, Zn speciation is minimally affected by aging HexB in the absence and presence of Mn(II), with a mixture of ^{IV}Zn and ^{VI}Zn occurring primarily as DC complexes.

Like HexB, Ni and Zn speciation on TriB exhibits only minor changes upon aging for 25 days at pH 7 (Figures 1,2). Ni binding mechanisms involve a mixture of TE and DC Ni surface complexes in the absence of added Mn(II), similar to Ni speciation after 40 hours of reaction

319 (Table S1). Aging with 0.75 mM Mn(II) suppresses DC surface complexes, with TE complexes
320 becoming the dominant (and perhaps sole) Ni species (Table S1). For Zn, the Fourier transform
321 feature at ~2.7 Å, indicative of TE complexes, is dampened during aging without Mn(II) but is
322 unaffected when 0.75 mM Mn(II) is present (Figure 2I). Fitting suggests that aging without
323 Mn(II) favors DC complexes over TE complexes, but that a mixture of such species are present
324 when TriB is aged with added Mn(II), similar to what is seen after Ni is adsorbed for 40 hours.
325

326 # 4. DISCUSSION

327 ## 4.1. Metal Binding Mechanisms Following Adsorption and Coprecipitation

328 These results show that Ni and Zn binding mechanisms are similar when reacted over
329 short (i.e., 40 hour) time scales via adsorption or coprecipitation with phyllomanganates, with the
330 exception that Ni may incorporate into the mineral structure. Vacancy content and pH are the
331 primary controls on Ni and Zn speciation. This is consistent with several prior studies, which
332 found that these metals bind as TC complexes onto high-vacancy materials like δ-MnO_2,[20,35,41,42]
333 with DC complexes forming under high metal loadings[35] and Ni incorporating into δ-MnO2 at
334 high pH,[35,42] and TE sorption onto low-vacancy TriB.[20,42] The presence of TC Ni and Zn
335 complexes on TriB at pH 4 but not at pH 7 suggests that a substantial vacancy content has
336 developed in this material under weakly acidic conditions. Previous research found that aging
337 TriB at pH 4 results in a reduction of Mn(III) content, the creation of sheet vacancies, and a
338 transition to hexagonal sheet symmetry, likely because acidic conditions promote Mn(III)
339 disproportionation reactions and exchange of Na^+ for H^+.[40,49,54,68] Kinetic experiments
340 investigating the conversion of triclinic birnessite to hexagonal birnessite at pH 4 suggest that
341 chemical equilibrium is reached within approximately 2 hours, with substantial release of Mn(II)

and Na^+ to solution within 1 minute.[49] Such rapid proton-promoted structural changes in TriB at low pH would explain the both the macroscopic Ni uptake and Mn release by TriB overnight at pH 4 as discussed in the SI (Figure S3) and the presence of both TC and incorporated Ni in the 40 hour TriB pH 4 samples. Previous observations that Ni incorporation into phyllomanganates increases with increasing pH[41] may, therefore, only apply to manganese oxides with substantial initial vacancy contents (e.g., δ-MnO_2 and HexB).

4.2. Mechanism of Mn(II)-Induced Metal Speciation Changes During Aging at pH 4

For most mineral-metal systems investigated, dissolved Mn(II) consistently promotes ^{IV}Zn over ^{VI}Zn surface species on phyllomanganates during aging at pH 4. As this change in coordination correlates with a shift from adsorption at vacancy sites (TC complexes) to sheet edges (DC complexes), it suggests that edge sites better stabilize ^{IV}Zn. This Mn(II)-induced shift from TC to DC complexes occurs for both adsorbed Ni and Zn. In the δ-MnO_2 system, the transition from predominantly TC to DC Ni and Zn only occurs at high Mn(II) loadings [(7.5 mM initial Mn(II)], while the transition for Ni occurs at lower Mn(II) loadings [(0.75 mM initial Mn(II)] in the HexB system. These speciation changes correlate with Mn(II)-induced rotational ordering and the formation of intermixed hexagonal and orthogonal sheets with long range ordering, which occur at lower Mn(II) loadings in the HexB system relative to the δ-MnO_2 system under similar experimental conditions.[40] Such observations suggest that phyllomanganate structural changes and competitive adsorption cause the altered Ni and Zn uptake and speciation. Edge-binding complexes like DC and TE species may be promoted by the formation of orthogonally symmetric phyllomanganate sheets, as these sheets have more structural Mn(III)

364 and fewer vacancies relative to hexagonally symmetric sheets,[54,74] and therefore possess fewer
365 binding sites for TC adsorption.

366 TriB shows distinct metal binding behavior at pH 4. The substantial Mn(III) component
367 of this phase undergoes extensive disproportionation,[40] producing dissolved Mn(II) (Table 1) and
368 vacancy-rich, rotationally ordered hexagonally-symmetric phyllomanganate sheets.[40] Previous
369 research has demonstrated that Ni and Zn also promote the formation of vacancy-rich
370 phyllomanganates by ejecting Mn(II) to solution,[18,20] presumably by promoting
371 disproportionation of Mn(III) in the sheet or capping vacancies through competitive binding. The
372 favorability of these vacancy-forming disproportionation reactions should decrease when the
373 product, aqueous Mn(II), is added to the system. This likely is the cause of decreased Ni and Zn
374 uptake in the presence of Mn(II), and may partially explain why less Ni and Zn bind to TriB than
375 to δ-MnO_2 or HexB at pH 4. The results indicate that Ni competes with Mn(II) for vacancy sites
376 more effectively than Zn, as Ni uptake is reduced only with a high dissolved Mn(II)
377 concentration (7.5 mM) but Zn uptake is inhibited at both Mn(II) concentrations studied. The
378 variability in the amount of Ni incorporated into TriB at pH 4 with increasing Mn(II)
379 concentration also likely relates to the changing favorability of Mn(III) disproportionation. Zn
380 behavior is more straightforward, as the shift from TC to DC complexes and decreasing uptake is
381 consistent with competitive adsorption between Zn and dissolved Mn(II).

382

383 **4.3. Mechanisms of Mn(II)-Induced Metal Speciation Changes During Aging at pH 7**

384 Unlike at pH 4, Ni and Zn speciation on phyllomanganates are largely unaffected by
385 aqueous Mn(II) during aging at pH 7. The slight decrease in Ni incorporation into δ-MnO_2 when
386 dissolved Mn(II) is present corresponds to an increase in structural Mn(III), and likely decrease

in vacancy content, observed in a past study under similar conditions.[40] With δ-MnO_2, changes in Zn coordination are primarily the result of aging, irrespective of Mn(II) concentration. Ni and Zn speciation in the HexB system is largely unaffected by the addition of Mn(II), consistent with the finding that Mn(II) does not alter the HexB structure at this pH value.[40] For TriB, Mn(II) addition results in a shift from DC to TE surface complexes for both Ni and Zn. One possible explanation for this promotion of TE over DC Ni and Zn complexes is that Mn(II) may simply outcompete these metals for DC adsorption sites. If this Mn(II)-metal competitive adsorption is in fact the cause for enhanced TE adsorption, there must be enough binding sites for TE complexes so that macroscopic metal uptake is unaffected. Alternatively, the increased proportion of Ni and Zn TE complexes when Mn(II) is added may result from Mn(II) adsorption to edge sites followed by comproportionation to form Mn(III),[39,40] as recent research shows that Mn(III) on sheet edges favors Ni TE over DC adsorption.[50]

4.4. Environmental Implications

This study shows that Mn(II) alters trace metal speciation in phyllomanganates, with differing effects at acidic and circumneutral pH. Trace metals such as Ni and Zn commonly coexist with phyllomanganates and aqueous Mn(II) in acid and coal mine drainage sites, marine sediments, and anoxic soils.[4,32,58-61,75,76] At acidic pH, Mn(II) redistributes Ni and Zn surface complexes from capping vacancies within the interlayer to binding at more exposed edge sites and, at high loadings, suppresses overall Ni and Zn uptake by the solid. The amount of Mn(II) remaining in solution at the end of these pH 4 high Mn(II) experiments [7.5 mM Mn(II)], although large, is within the same order of magnitude for dissolved Mn(II) concentrations in highly contaminated coal mine drainage sites.[32,58] Thus, phyllomanganates may not sequester

trace metals as effectively in acidic soils and acid or coal mine drainage sites with appreciable concentrations of aqueous Mn(II). In more alkaline marine sediments or calcareous coal mine drainage sites, Mn(II) may serve to alter the long-term behavior of incorporated metals, such as Ni, in phyllomanganates with high initial vacancy contents. In fact, the heavy metal content of phyllomanganates in a karst cave system has been shown to inversely correlate with dissolved Mn(II) concentrations, potentially caused by decreased sheet vacancy content following Mn(II) uptake.[3] These results demonstrate that Mn(II)-bearing fluids will alter trace metal uptake and speciation on phyllomanganates in aquatic and soil systems.

5. ASSOCIATED CONTENT

Supporting Information. This document contains information regarding mineral and reagent preparation, details of the fitting routines for the EXAFS spectra, characterization of the synthesized phyllomanganates, and a discussion regarding alternative EXAFS spectral fits. The SI document also includes figures of the Ni and Zn EXAFS spectra and model fits and tables of the Langmuir isotherm fit parameters (for the Ni overnight adsorption isotherms), the Ni and Zn EXAFS fitting parameters, and tables comparing final and alternate EXAFS fitting parameters for the Ni and Zn systems. This information is available free of charge via the Internet at http://pubs.acs.org.

6. AUTHOR INFORMATION

Corresponding Author Margaret A. G. Hinkle now at:

* Department of Mineral Sciences, Smithsonian Institution, National Museum of Natural History, Washington, DC 20560 Tel: +1-202-633-1815; E-mail: mhinkle@eps.wustl.edu

[†]Katherine G. Dye now at: Ocean Research College Academy, Everett, WA 98201

Author Contributions

The manuscript was written through contributions by Margaret A.G. Hinkle and Jeffrey G. Catalano. Katherine G. Dye synthesized metal coprecipitated manganese oxides and performed acid digestions on those materials to determine total mol % Ni and Zn. All authors have given approval for the final version of the manuscript.

Notes

The authors declare no competing financial interest.

7. ACKNOWLEDGEMENTS

This research was supported by the U.S. National Science Foundation (NSF), Division of Earth Sciences, Geobiology and Low-Temperature Geochemistry Program with Grant No. EAR-1056480. ICP-OES analyses were conducted at the Nano Research Facility at Washington University, which is supported through NSF Award No. ECS-0335765. XAFS spectra were collected at beamline 20-BM-B at the APS, an Office of Science User Facility run by the U.S. Department of Energy (DOE) Office of Science by Argonne National Laboratory, supported by the U.S. DOE through Contract No. DE-AC02-06CH11357 and at beamline 4-1 at SSRL, operated by SLAC National Accelerator Laboratory with support from the DOE Office of Science through Contract No. DE-AC02-76SF00515. XRD patterns were collected with the Bruker D8 Advance XRD instrument at Washington University in St. Louis, supported by the NSF through Award No. EAR-1161543. We particularly thank Dale Brewe, John Bargar, and Ryan Davis for their support in collecting XAFS spectra. We also especially thank Elaine D. Flynn, for collecting ICP-OES data on the 40-hour sample filtrates.

8. REFERENCES

(1) Singh, A. K.; Hasnain, S. I.; and Banerjee, D. K. Grain size and geochemical partitioning of heavy metals in sediments of the Damodar River--a tributary of the lower Ganga, India. *Environ. Geo.* **1999**, *39*, 90-98.

(2) Li, X.; Shen, Z.; Wai, O. W. H.; and Li, Y. Z. Chemical forms of Pb, Zn and Cu in the sediments profiles of the Pearl River Estuary. *Mar. Pollut. Bull.* **2001**, *42.*

(3) Frierdich, A. J. and Catalano, J. G. Distribution and speciation of trace elements in iron and manganese oxide cave deposits. *Geochim. Cosmochim. Acta.* **2012**, *91*, 240-253.

(4) Tebo, B. M.; Bargar, J. R.; Clement, B. G.; Dick, G. J.; Murray, K. J.; Parker, D.; Verity, R.; and Webb, S. M. Biogenic manganese oxides: Properties and mechanisms of formation. *Annu. Rev. Earth Pl. Sc.* **2004**, *32*, 287-328.

(5) Goldberg, E. D. Marine Geochemistry 1. Chemical scavengers of the sea. *J. Geol.* **1954**, *62*, 249-265.

(6) Miyata, N.; Tani, Y.; Sakata, M.; and Iwahori, K. Microbial manganese oxide formation and interaction with toxic metal ions. *J. Biosci. Bioeng.* **2007**, *104*, 1-8.

(7) Brown, G. E. and Parks, G. A. Sorption of trace elements on mineral surfaces: Modern perspectives from spectroscopic studies, and comments on sorption in the marine environment. *Int. Geol. Rev.* **2001**, *43*, 963-1073.

(8) White, W. B.; Vito, C.; and Scheetz, B. E. The mineralogy and trace element chemistry of black manganese oxide deposits from caves. *J. Cave Karst Stud.* **2009**, *71*, 136-143.

(9) Jenne, E. A. In *Advances in Chemistry*; American Chemical Society, 1968; p. 337-387.

(10) Tebo, B. M.; Ghiorse, W. C.; van Waasbergen, L. G.; Siering, P. L.; and Caspi, R. Bacterially mediated mineral formation; insights into manganese (II) oxidation from molecular genetic and biochemical studies. *Rev. Mineral. Geochem.* **1997**, *35*, 225-266.

(11) Manceau, A.; Tamura, N.; Marcus, M. A.; MacDowell, A. A.; Celestre, R. S.; Sublett, R. E.; Sposito, G.; and Padmore, H. A. Deciphering Ni sequestration in soil ferromanganese nodules by combining X-ray fluorescence, absorption, and diffraction at micrometer scales of resolution. *Am. Mineral.* **2002**, *87*, 1494-1499.

(12) Manceau, A.; Lanson, M.; and Takahashi, Y. Mineralogy and crystal chemistry of Mn, Fe, Co, Ni, and Cu in a deep-sea Pacific polymetallic nodule. *Am. Mineral.* **2014**, *99*, 2068-2083.

(13) Lanson, B.; Marcus, M. A.; Fakra, S.; Panfili, F.; Geoffroy, N.; and Manceau, A. Formation of Zn-Ca phyllomanganate nanoparticles in grass roots. *Geochim. Cosmochim. Acta.* **2008**, *72*, 2478-2490.

(14) Siegel, M. D. and Turner, S. Crystalline todorokite associated with biogenic debris in manganese nodules. *Science.* **1983**, *219*, 172-174.

(15) Post, J. E. Manganese oxide minerals: Crystal structures and economic and environmental significance. *Proc. Natl. Acad. Sci. U. S. A.* **1999**, *96*, 3447-3454.

(16) Villalobos, M.; Escobar-Quiroz, I. N.; and Salazar-Camacho, C. The influence of particle size and structure on the sorption and oxidation behavior of birnessite: I. Adsorption of As(V) and oxidation of As(III). *Geochim. Cosmochim. Acta.* **2014**, *125*, 564-581.

(17) Yin, H.; Tan, W.; Zheng, L.; Cui, H.; Qiu, G.; Liu, F.; and Feng, X. Characterization of Ni-rich hexagonal birnessite and its geochemical effects on aqueous Pb^{2+}/Zn^{2+} and As(III). *Geochim. Cosmochim. Acta.* **2012**, *93*, 47-62.

(18) Grangeon, S.; Manceau, A.; Guilhermet, J.; Gaillot, A. C.; Lanson, M.; and Lanson, B. Zn sorption modifies dynamically the layer and interlayer structure of vernadite. *Geochim. Cosmochim. Acta.* **2012**, *85*, 302-313.

(19) Boonfueng, T.; Axe, L.; Yee, N.; Hahn, D.; and Ndiba, P. K. Zn sorption mechanisms onto sheathed *Leptothrix discophora* and the impact of the nanoparticulate biogenic Mn oxide coating. *J. Colloid Interface Sci.* **2009**, *333*, 439-447.

(20) Zhu, M.; Ginder-Vogel, M.; and Sparks, D. L. Ni(II) sorption on biogenic Mn-oxides with varying Mn octahedral layer structure. *Environ. Sci. Technol.* **2010**, *44*, 4472-4478.

(21) Zhu, M.; Ginder-Vogel, M.; Parikh, S. J.; Feng, X. H.; and Sparks, D. L. Cation effects on the layer structure of biogenic Mn-oxides. *Environ. Sci. Technol.* **2010**, *44*, 4465-4471.

(22) Yu, Q.; Sasaki, K.; Tanaka, K.; Ohnuki, T.; and Hirajima, T. Zinc sorption during bio-oxidation and precipitation of manganese modifies the layer stacking of biogenic birnessite. *Geomicrobiol. J.* **2013**, *30*, 829-839.

(23) Cai, J.; Liu, J.; and Suib, S. L. Preparative parameters and framework dopant effects in the synthesis of layer-structure birnessite by air oxidation. *Chem. Mater.* **2002**, *14*, 2071-2077.

(24) Paterson, E.; Bunch, J. L.; and Clark, D. R. Cation exchange in synthetic manganates: I. Alkylammonium exchange in a synthetic phyllomanganate. *Clay Miner.* **1986**, *21*, 949-955.

(25) Shen, Y. -F.; Suib, S. L.; and O'Young, C. -L. Effects of inorganic cation templates on octahedral molecular sieves of manganese oxide. *J. Am. Chem. Soc.* **1994**, *116*, 11020-11029.

(26) Bodeï, S.; Manceau, A.; Geoffroy, N.; Baronnet, A.; and Buatier, M. Formation of todorokite from vernadite in Ni-rich hemipelagic sediments. *Geochim. Cosmochim. Acta.* **2007**, *71*, 5698-5716.

(27) Ching, S.; Krukowska, K. S.; and Suib, S. L. A new synthetic route to todorokite-type manganese oxides. *Inorg. Chim. Acta.* **1999**, *294*, 123-132.

(28) Lefkowitz, J. P.; Rouff, A. A.; and Elzinga, E. J. Influence of pH on the reductive transformation of birnessite by aqueous Mn(II). *Environ. Sci. Technol.* **2013**, *47*, 10364-10371.

(29) Elzinga, E. J. and Kustka, A. B. A Mn-54 radiotracer study of Mn isotope solid-liquid exchange during reductive transformation of vernadite (δ-MnO2) by aqueous Mn (II). *Environ. Sci. Technol.* **2015**, *49*, 4310-4316**.**

(30) Elzinga, E. J. Reductive transformation of birnessite by aqueous Mn (II). *Environ. Sci. Technol.* **2011**, *45*, 6366-6372.

(31) Lefkowitz, J. P. and Elzinga, E. J. Impacts of Aqueous Mn(II) on the Sorption of Zn(II) by Hexagonal Birnessite.. *Environ. Sci. Technol.* **2015**, *49*, 4886-4893.

(32) Tan, H.; Zhang, G.; Heaney, P. J.; Webb, S. M.; and Burgos, W. D. Characterization of manganese oxide precipitates from Appalachian coal mine drainage treatment systems. *Appl. Geochem.* **2010**, *25*, 389-399.

(33) Dick, G. J.; Clement, B. G.; Webb, S. M.; Fodrie, F. J.; Bargar, J. R.; and Tebo, B. M. Enzymatic microbial Mn(II) oxidation and Mn biooxide production in the Guaymas Basin deep-sea hydrothermal plume. *Geochim. Cosmochim. Acta.* **2009**, *73*, 6517-6530.

(34) Manceau, A.; Kersten, M.; Marcus, M. A.; Geoffroy, N.; and Granina, L. Ba and Ni speciation in a nodule of binary Mn oxide phase composition from Lake Baikal. *Geochim. Cosmochim. Acta.* **2007**, *71*, 1967-1981.

(35) Manceau, A.; Lanson, M.; and Geoffroy, N. Natural speciation of Ni, Zn, Ba, and As in ferromanganese coatings on quartz using X-ray fluorescence, absorption, and diffraction. *Geochim. Cosmochim. Acta.* **2007**, *71*, 95-128.

(36) Friedl, G.; Wehrli, B.; and Manceau, A. Solid phases in the cycling of manganese in eutrophic lakes: New insights from EXAFS spectroscopy. *Geochim. Cosmochim. Acta.* **1997**, *61*, 275-290.

(37) Wehrli, B.; Friedl, G.; and Manceau, A. Reaction rates and products of manganese oxidation at the sediment-water interface. In *Advances in Chemistry*; 1995; p. 111-134.

(38) Bargar, J. R.; Tebo, B. M.; Bergmann, U.; Webb, S. M.; Glatzel, P.; Chiu, V. Q.; and Villalobos, M. Biotic and abiotic products of Mn(II) oxidation by spores of the marine *Bacillus sp.* strain SG-1. *Am. Mineral.* **2005**, *90*, 143-154.

(39) Zhao, H.; Zhu, M.; Li, W.; Elzinga, E. J.; Villalobos, M.; Liu, F.; Zhang, J.; Feng, X.; and Sparks, D. L. Redox Reactions between Mn(II) and Hexagonal Birnessite Change Its Layer Symmetry.. *Environ. Sci. Technol.* **2016**, *50*, 1750-8.

(40) Hinkle, M. A. G.; Flynn, E.; and Catalano, J. G. Effect of Mn(II) on manganese oxide sheet structures. *Geochim. Cosmochim. Acta.* **2016**, *192*, 220-234.

(41) Peacock, C. L. Physiochemical controls on the crystal-chemistry of Ni in birnessite: Genetic implications for ferromanganese precipitates. *Geochim. Cosmochim. Acta.* **2009**, *73*, 3568-3578.

(42) Peacock, C. L. and Sherman, D. M. Sorption of Ni by birnessite: Equilibrium controls on Ni in seawater. *Chem. Geol.* **2007**, *238*, 94-106.

(43) Peacock, C. L. and Sherman, D. M. Crystal-chemistry of Ni in marine ferromanganese crusts and nodules. *Am. Mineral.* **2007**, *92*, 1087-1092.

(44) Toner, B.; Manceau, A.; Webb, S. M.; and Sposito, G. Zinc sorption by biogenic hexagonal birnessite particles within a hydrated bacterial biofilm. *Geochim. Cosmochim. Acta.* **2006**, *70*, 27-43.

(45) Manceau, A.; Tommaseo, C.; Rihs, S.; Geoffroy, N.; Chateigner, D.; Schlegel, M.; Tisserand, D.; Marcus, M. A.; Tamura, N.; and Chen, Z. -S. Natural speciation of Mn, Ni, and Zn at the micrometer scale in a clayey paddy soil using X-ray fluorescence, absorption, and diffraction. *Geochim. Cosmochim. Acta.* **2005**, *69*, 4007-4034.

(46) Marcus, M. A.; Manceau, A.; and Kersten, M. Mn, Fe, Zn and As speciation in a fast-growing ferromanganese marine nodule. *Geochim. Cosmochim. Acta.* **2004**, *68*, 3125-3136.

(47) Manceau, A.; Tamura, N.; Celestre, R. S.; MacDowell, A. A.; Geoffroy, N.; Sposito, G.; and Padmore, H. A. Molecular-scale speciation of Zn and Ni in soil ferromanganese nodules from loess soils of the Mississippi Basin. *Environ. Sci. Technol.* **2002**, *37*, 75-80.

(48) Manceau, A.; Drits, V. A.; Silvester, E.; Bartoli, C.; and Lanson, B. Structural mechanism of Co^{2+} oxidation by the phyllomanganate buserite. *Am. Mineral.* **1997**, *82*, 1150-1175.

(49) Silvester, E.; Manceau, M.; and Drits, V. A. Structure of synthetic monoclinic Na-rich birnessite and hexagonal birnessite: II. Results from chemical studies and EXAFS spectroscopy. *Am. Mineral.* **1997**, *82*, 962-978.

(50) Simanova, A. A.; Kwon, K. D.; Bone, S. E.; Bargar, J. R.; Refson, K.; Sposito, G.; and Peña, J. Probing the sorption reactivity of the edge surfaces in birnessite nanoparticles using nickel(II). *Geochim. Cosmochim. Acta.* **2015**, *164*, 191-204.

(51) van Genuchten, C. M. and Peña, J. Sorption selectivity of birnessite particle edges: a d-PDF analysis of Cd(II) and Pb(II) sorption by δ-MnO_2 and ferrihydrite.. *Environ Sci Process Impacts.* **2016**, *18*, 1030-41.

(52) Simanova, A. A. and Peña, J. Time-resolved investigation of cobalt oxidation by Mn(III)-rich δ-MnO_2 using quick X-ray absorption spectroscopy. *Environ. Sci. Technol.* **2015**, *49*, 10867-10876.

(53) Peña, J.; Bargar, J. R.; and Sposito, G. Copper sorption by the edge surfaces of synthetic birnessite nanoparticles. *Chem. Geol.* **2015**, *396*, 196-207.

(54) Lanson, B.; Drits, V. A.; Silvester, E.; and Manceau, A. Structure of H-exchanged hexagonal birnessite and its mechanism of formation from Na-rich monoclinic buserite at low pH. *Am. Mineral.* **2000**, *85*, 826-838.

(55) Peña, J.; Kwon, K. D.; Refson, K.; Bargar, J. R.; and Sposito, G. Mechanisms of nickel sorption by a bacteriogenic birnessite. *Geochim. Cosmochim. Acta.* **2010**, *74*, 3076-3089.

(56) Lopano, C. L.; Heaney, P. J.; Post, J. E.; Hanson, J.; and Komarneni, S. Time-resolved structural analysis of K- and Ba-exchange reactions with synthetic Na-birnessite using synchrotron X-ray diffraction. *Am. Mineral.* **2007**, *92*, 380-387.

(57) Villalobos, M.; Toner, B.; Bargar, J. R.; and Sposito, G. Characterization of the manganese oxide produced by *pseudomonas putida* strain MnB1. *Geochim. Cosmochim. Acta.* **2003**, *67*, 2649-2662.

(58) Luan, F.; Santelli, C. M.; Hansel, C. M.; and Burgos, W. D. Defining manganese(II) removal processes in passive coal mine drainage treatment systems through laboratory incubation experiments. *Appl. Geochem.* **2012**, *27*, 1567-1578.

(59) Mayanna, S.; Peacock, C. L.; Schäffner, F.; Grawunder, A.; Merten, D.; Kothe, E.; and Büchel, G. Biogenic precipitation of manganese oxides and enrichment of heavy metals at acidic soil pH. *Chem. Geol.* **2015**, *402*, 6-17.

(60) Kay, J. T.; Conklin, M. H.; Fuller, C. C.; and O'Day, P. A. Processes of nickel and cobalt uptake by a manganese oxide forming sediment in Pinal Creek, Globe Mining District, Arizona. *Environ. Sci. Technol.* **2001**, *35*, 4719-4725.

(61) Cravotta III, C. A. Dissolved metals and associated constituents in abandoned coal-mine discharges, Pennsylvania, USA. Part 1: Constituent quantities and correlations. *Appl. Geochem.* **2008**, *23*, 166-202.

(62) Ravel, B. and Newville, M. ATHENA, ARTEMIS, HEPHAESTUS: Data analysis for X-ray absorption spectroscopy using IFEFFIT. *J. Synchrotron Radiat.* **2005**, *12*, 537-541.

(63) Newville, M. IFEFFIT: interactive EXAFS analysis and FEFF fitting. *J. Synchrotron Radiat.* **2001**, *8*, 322-324.

(64) Webb, S. M. SIXPack: A Graphical User Interface for XAS Analysis using IFEFFIT. *Phys. Scripta.* **2005**, *T115*, 1011-1014.

(65) Post, J. E. and Appleman, D. E. Chalcophanite, ZnMn3O7-3H2O: New crystal-structure determinations. *Am. Mineral.* **1988**, *73*, 1401-1404.

(66) Rehr, J. J.; Kas, J. J.; Vila, F. D.; Prange, M. P.; and Jorissen, K. Parameter-free calculations of X-ray spectra with FEFF9. *Phys. Chem. Chem. Phys.* **2010**, *12*, 5503-5513.

(67) Ling, F. T.; Heaney, P. J.; Post, J. E.; and Gao, X. Transformations from triclinic to hexagonal birnessite at circumneutral pH induced through pH control by common biological buffers. *Chem. Geol.* **2015**, *416*, 1-10.

(68) Drits, V. A.; Silvester, E.; Gorshkov, A. I.; and Manceau, A. Structure of synthetic monoclinic Na-rich birnessite and hexagonal birnessite: I. Results from X-ray diffraction and selected-area electron diffraction. *Am. Mineral.* **1997**, *82*, 946-961.

(69) Manceau, A.; Marcus, M. A.; Grangeon, S.; Lanson, M.; Lanson, B.; Gaillot, A. -C.; Skanthakumar, S.; and Soderholm, L. Short-range and long-range order of phyllomanganate nanoparticles determined using high-energy X-ray scattering. *J. Appl. Crystallogr.* **2013**, *46*, 193-209.

(70) Manceau, A.; Lanson, B.; and Drits, V. A. Structure of heavy metal sorbed birnessite. Part III: Results from powder and polarized extended X-ray absorption fine structure spectroscopy. *Geochim. Cosmochim. Acta.* **2002**, *66*, 2639-2663.

(71) Lanson, B.; Drits, V. A.; Gaillot, A. -C.; Silvester, E.; Plançon, A.; and Manceau, A. Structure of heavy-metal sorbed birnessite: Part 1. Results from X-ray diffraction. *Am. Mineral.* **2002**, *87*, 1631-1645.

(72) Fuller, C. C. and Bargar, J. R. Processes of zinc attenuation by biogenic manganese oxides forming in the hyporheic zone of Pinal Creek, Arizona. *Environ. Sci. Technol.* **2014**, *48*, 2165-2172.

(73) Kwon, K. D.; Refson, K.; and Sposito, G. Understanding the trends in transition metal sorption by vacancy sites in birnessite. *Geochim. Cosmochim. Acta.* **2013**, *101*, 222-232.

(74) Drits, V. A.; Lanson, B.; and Gaillot, A. -C. Birnessite polytype systematics and identification by powder X-ray diffraction. *Am. Mineral.* **2007**, *92*, 771-788.

(75) Tebo, B. M.; Johnson, H. A.; McCarthy, J. K.; and Templeton, A. S. Geomicrobiology of manganese(II) oxidation. *Trends Microbiol.* **2005**, *13*, 421-428.

(76) Graybeal, A. L. and Heath, G. R. Remobilization of transition metals in surficial pelagic sediments from the eastern Pacific. *Geochim. Cosmochim. Acta.* **1984**, *48*, 965-975.

664 **Table 1.** pH 4 sample abbreviations and conditions.

Sample ID[a]	Mn Oxide	Reaction Time	$[Mn]_{init}$ (mmol L^{-1})	$[Mn]_{soln}$ (mmol L^{-1})	$[Mn]_{ads}$ (mmol g^{-1})	$[Me]_{soln}$ (mmol L^{-1})	$[Me]_{ads}$ (mmol g^{-1})
Ni(II):							
4δad	δ-MnO_2	40 hours	0	BDL[b]	-[c]	BDL	0.092
4δno	δ-MnO_2	25 days	0	BDL	-	BDL	0.092
4δlo	δ-MnO_2	25 days	0.75	BDL	0.30	BDL	0.092
4δhi	δ-MnO_2	25 days	7.5	3.4 ± 0.2	1.64	BDL	0.092
4HBad	HexB	40 hours	0	BDL	-	BDL	0.092
4HBno	HexB	25 days	0	BDL	-	BDL	0.092
4HBlo	HexB	25 days	0.75	0.106 ± 0.006	0.26	0.018 ± 0.006	0.085
4HBhi	HexB	25 days	7.5	5.7 ± 0.1	0.72	0.16 ± 0.01	0.028
4TBad	TriB	40 hours	0	0.154 ± 0.001	-0.06[d]	BDL	0.092
4TBno	TriB	25 days	0	0.42 ± 0.01	-0.17	0.060 ± 0.008	0.068
4TBlo	TriB	25 days	0.75	0.87 ± 0.01	-0.05	0.059 ± 0.007	0.068
4TBhi	TriB	25 days	7.5	6.9 ± 0.2	0.24	0.11 ± 0.005	0.048
Zn(II):							
4δad	δ-MnO_2	40 hours	0	BDL	-	BDL	0.092
4δno	δ-MnO_2	25 days	0	0.034 ± 0.005	-0.01	BDL	0.092
4δlo	δ-MnO_2	25 days	0.75	BDL	0.30	BDL	0.092
4δhi	δ-MnO_2	25 days	7.5	4.29 ± 0.07	1.28	0.217 ± 0.008	0.005
4HBad	HexB	40 hours	0	0.011 ± 0.003	0.00	BDL	0.092
4HBno	HexB	25 days	0	0.006 ± 0.005	0.00	BDL	0.092
4HBlo	HexB	25 days	0.75	0.084 ± 0.008	0.27	0.036 ± 0.01	0.078
4HBhi	HexB	25 days	7.5	5.7 ± 0.2	0.72	0.21 ± 0.01	0.008
4TBad	TriB	40 hours	0	0.133 ± 0.002	-0.05	BDL	0.092
4TBno	TriB	25 days	0	0.429 ± 0.007	-0.17	0.038 ± 0.008	0.077
4TBlo	TriB	25 days	0.75	1.02 ± 0.01	-0.11	0.072 ± 0.006	0.063
4TBhi	TriB	25 days	7.5	6.6 ± 0.1	0.36	0.181 ± 0.008	0.020

665 [a] Sample IDs as used in figures. Additional sample IDs not included in this table are 'co-δ,' 'co-HB,' and
666 'co-TB' for Ni or Zn coprecipitated with δ-MnO_2, HexB, or TriB, respectively.
667 [b] BDL denotes any samples with $[Ni]_{soln}$, $[Zn]_{soln,}$ or $[Mn]_{soln}$ below detection limit (0.006 mM; 0.035 mM;
668 and 0.006 mM, respectively).
669 [c] (-) Denotes no aqueous Mn(II) added to the sample and dissolved Mn(II) is BDL so this parameter is not
670 reported.
671 [d] Negative values indicate net release of Mn(II) to solution.
672

673
674 **Table 2.** pH 7 sample abbreviations and conditions.

Sample ID[a]	Mn Oxide	Reaction Time	$[Mn]_{init}$ (mmol L^{-1})	$[Mn]_{soln}$ (mmol L^{-1})	$[Mn]_{ads}$ (mmol g^{-1})	$[Me]_{soln}$ (mmol L^{-1})	$[Me]_{ads}$ (mmol g^{-1})
Ni(II):							
7δad	δ-MnO_2	40 hours	0	BDL[b]	-[c]	BDL	0.092
7δno	δ-MnO_2	25 days	0	BDL	-	BDL	0.092
7δlo	δ-MnO_2	25 days	0.75	BDL	0.30	BDL	0.092
7HBad	HexB	40 hours	0	BDL	-	BDL	0.092
7HBno	HexB	25 days	0	BDL	-	BDL	0.092
7HBlo	HexB	25 days	0.75	BDL	0.30	BDL	0.092
7TBad	TriB	40 hours	0	BDL	-	BDL	0.092
7TBno	TriB	25 days	0	BDL	-	BDL	0.092
7TBlo	TriB	25 days	0.75	0.023 ± 0.006	0.29	BDL	0.092
Zn(II):							
7δad	δ-MnO_2	40 hours	0	0.007 ± 0.001	0.00	BDL	0.092
7δno	δ-MnO_2	25 days	0	BDL	-	BDL	0.092
7δlo	δ-MnO_2	25 days	0.75	BDL	0.30	BDL	0.092
7HBad	HexB	40 hours	0	BDL	-	BDL	0.092
7HBno	HexB	25 days	0	BDL	-	BDL	0.092
7HBlow	HexB	25 days	0.75	BDL	0.30	BDL	0.092
7TBad	TriB	40 hours	0	BDL	-	BDL	0.092
7TBno	TriB	25 days	0	BDL	-	BDL	0.092
7TBlo	TriB	25 days	0.75	BDL	0.30	BDL	0.092

675 [a] Sample IDs as used in figures. Additional sample IDs not included in this table are 'co-δ,' 'co-HB,' and
676 'co-TB' for Ni or Zn coprecipitated with δ-MnO_2, HexB, or TriB, respectively.
677 [b] BDL denotes any samples with $[Ni]_{soln}$, $[Zn]_{soln,}$ or $[Mn]_{soln}$ below detection limit (0.006 mM; 0.035 mM;
678 and 0.006 mM, respectively).
679 [c] (-) Denotes no aqueous Mn(II) added to the sample and dissolved Mn(II) is BDL so this parameter is not
680 reported.
681

682 **FIGURE CAPTIONS**
683
684 **Figure 1.** Ni K-edge XAFS spectra of Ni coprecipitated and reacted with δ-MnO_2 (A,B,C), HexB
685 (D,E,F), and TriB (G,H,I) (see Tables 1 and 2 for specific conditions). Diagnostic features at 2.5,
686 2.7 and 3.1 Å (R + ΔR) in R space (corresponding to Ni-Mn shells for incorporated Ni at 2.88 Å,
687 TE Ni at 3.08 Å, and DC/TC Ni at 3.48 Å, respectively) are denoted by dark blue vertical lines.
688
689 **Figure 2.** Zn K-edge XAFS spectra of Zn coprecipitated and reacted with δ-MnO_2 (A,B,C),
690 HexB (D,E,F), and TriB (G,H,I) (see Tables 1 and 2 for specific conditions). Diagnostic features
691 at 3.8 and 6.1 $Å^{-1}$ in k space (corresponding to ^{VI}Zn; features are shifted to the right for ^{IV}Zn) and
692 at 1.64, 2.7 Å and 3.1 Å (R + ΔR) in R space (corresponding to the Zn-O shell for ^{VI}Zn at 2.08
693 Å, Zn-Mn shell for TE Zn at 3.1 Å, and Zn-Mn shell for DC/TC Zn at 3.48 Å, respectively) are
694 denoted by dark blue vertical lines.
695
696
697
698

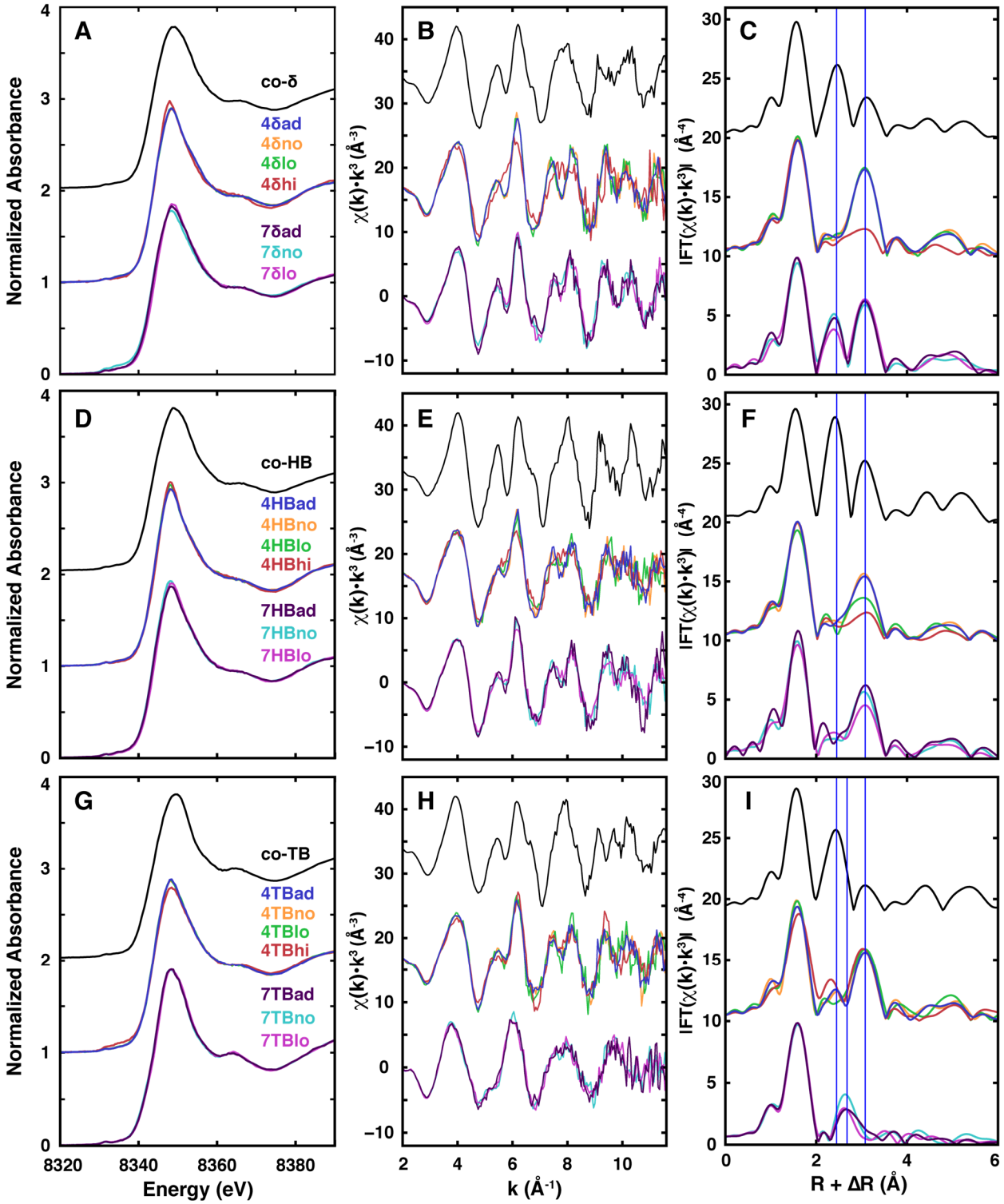

Figure 1. Ni K-edge XAFS spectra of Ni coprecipitated and reacted with δ-MnO_2 (A,B,C), HexB (D,E,F), and TriB (G,H,I) (see Tables 1 and 2 for specific conditions). Diagnostic features at 2.5, 2.7 and 3.1 Å (R + ΔR) in R space (corresponding to Ni-Mn shells for incorporated Ni at 2.88 Å, TE Ni at 3.08 Å, and DC/TC Ni at 3.48 Å, respectively) are denoted by dark blue vertical lines.

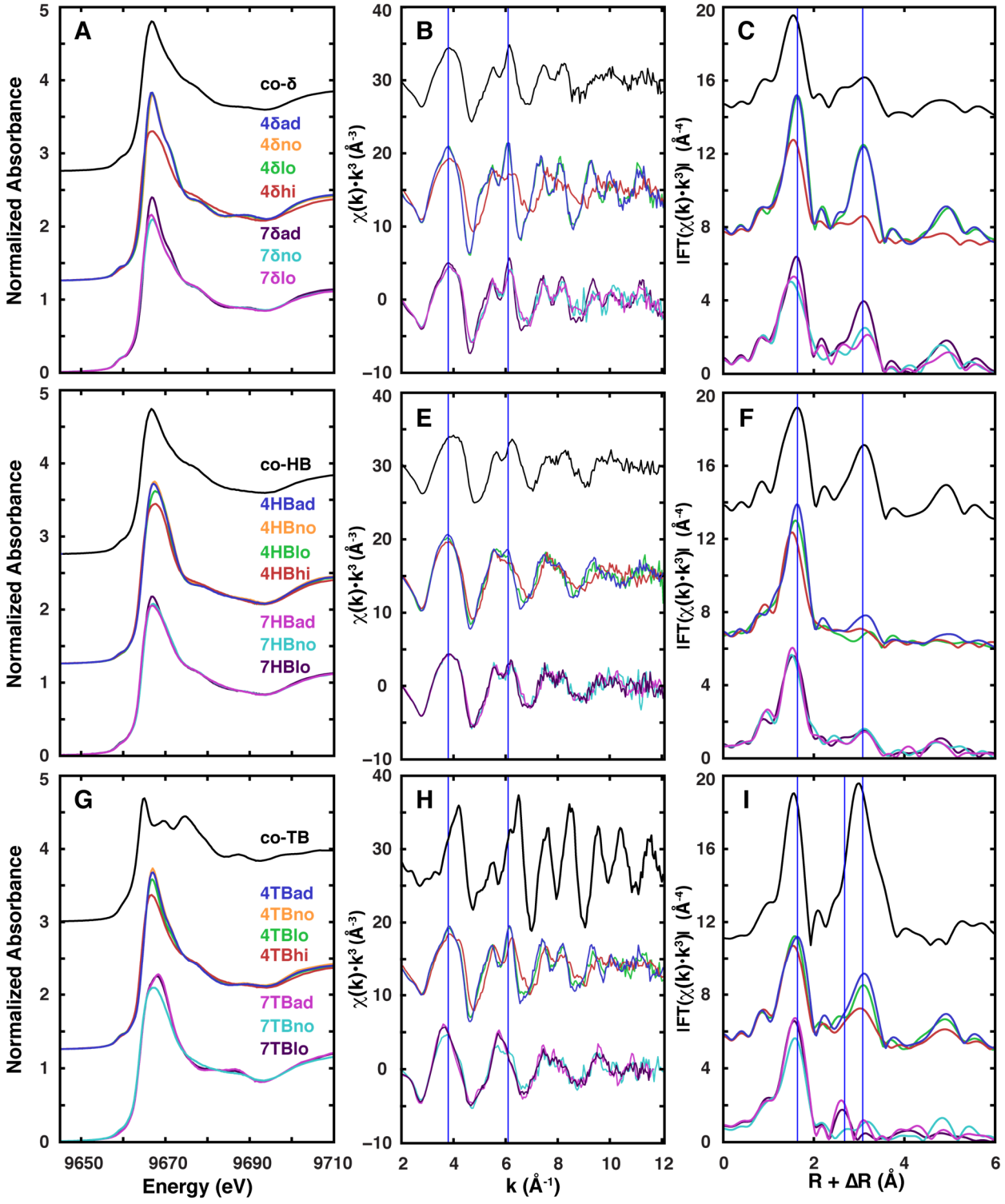

706
707 **Figure 2.** Zn K-edge XAFS spectra of Zn coprecipitated and reacted with δ-MnO_2 (A,B,C),
708 HexB (D,E,F), and TriB (G,H,I) (see Tables 1 and 2 for specific conditions). Diagnostic features
709 at 3.8 and 6.1 $Å^{-1}$ in k space (corresponding to ^{VI}Zn; features are shifted to the right for ^{IV}Zn) and
710 at 1.64, 2.7 Å and 3.1 Å (R + ΔR) in R space (corresponding to the Zn-O shell for ^{VI}Zn at 2.08
711 Å, Zn-Mn shell for TE Zn at 3.1 Å, and Zn-Mn shell for DC/TC Zn at 3.48 Å, respectively) are
712 denoted by dark blue vertical lines.

713 **TOC/ABSTRACT ART**

714